A Low-Complexity Artificial Neural Network-Based Optimal Droop Gain Design Strategy for DC Microgrids Onboard the More Electric Aircraft

Habibu Hussaini, Tao Yang, *Senior Member, IEEE*, Ge Bai, *Graduate Student Member, IEEE*, Matías Urrutia-Ortiz, and Serhiy Bozhko, *Senior Member, IEEE*

***Abstract*—This article proposes a new droop control design method based on a "reversed data training" of artificial neural network (ANN). Conventionally, after data collection, the ANN is used for forward mapping the control variables (inputs) and system response (outputs). After training, the ANN model can be used for optimal control design for each specific system performance requirement either through curve fittings or other optimization methods. In our proposed method, however, a reversed data training process is used. The ANN uses system responses as its inputs and control variables as outputs. By doing so, the ANN can identify the requested control variables directly for a given system performance request. In the example aircraft DC microgrid, multiple generation systems feed a common DC bus with droop control implemented. During the data-generating process, different droop coefficient combinations are used, and the resulting power sharing ratios are stored as outputs. However, the ANN is data reversely trained with power sharing ratios as inputs and droop coefficients being the outputs. Through this example, we have shown that the proposed approach is straightforward and effective to derive the optimal droop gains based on desired power sharing requests. The proposed approach is tested in both simulation and experiment.**

***Index Terms*—Computation, droop coefficient, droop control, converters, more electric aircraft, neural network, optimization**

This work was supported by the Clean Sky 2 Joint Undertaking through the European Union's Horizon 2020 Research and Innovation Programme under Grant 807081. The work of Habibu Hussaini was supported by the stipend funding from Petroleum Technology Development Fund (PTDF), Nigeria. (*Corresponding author: Tao Yang*.)

Habibu Hussaini is with the Power Electronics, Machines and Control Group, University of Nottingham, Nottingham NG7 2RD, U.K, and with the Department of Electrical and Electronics Engineering, Federal University of Technology, Minna, P.M.B. 65, 920101, Minna, Niger, Nigeria. (email: Habibu.Hussaini@nottingham.ac.uk, habufarid@futminna.edu.ng).

Tao Yang, Ge Bai, and Serhiy Bozhko are with the Power Electronics, Machines and Control Group, The University of Nottingham, Nottingham NG7 2RD, U.K. (emails: Tao.Yang@nottingham.ac.uk; Ge.Bai@nottingham.ac.uk, Serhiy.Bozhko@nottingham.ac.uk).

Matías Urrutia, is with print Electric Limited, Peregrine House, Ford Lane, West Sussex, BN18 0DF, UK. (email: matias.urrutia@sprint-electric.com)

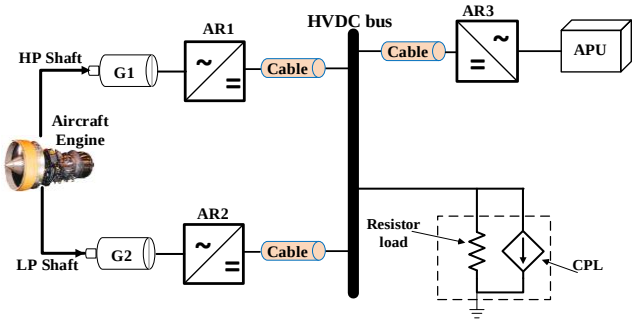

Fig. 1 Single bus EPS architecture candidate for future MEA application

I. Introduction

THE single-bus DC microgrid (MG) is considered a promising electrical power system (EPS) solution for various applications including the more electric aircraft (MEA). In this MG configuration, multiple power generation sources are interconnected in parallel to a shared DC bus using interfacing power electronic converters (PECs), as depicted in Fig. 1. The effective control and management of these power sources, as well as the regulation of the DC bus voltages, are achieved through the utilization of these interconnected PECs [1]. Numerous strategies have been proposed in recent studies to address the power sharing control challenges in such DC MGs [2]. The droop control method is one of the most widely employed methods among them. However, practical factors such as mismatched line impedance and offset in nominal voltage reference impact the accuracy of load sharing and the performance of voltage regulation. In the droop control mechanism, there is typically a trade-off between power sharing accuracy and voltage regulation. Increasing the droop gain can improve power sharing accuracy, but it may lead to poorer voltage regulation. Hence, the droop gain of converters plays an important role in determining the effectiveness of the droop control method. To improve its performance, it is necessary to explore new approaches and employ intelligent optimization

techniques.

The design and calculation of the optimal droop gains for converters represent a clever approach to improve the performance of the droop control method, without compromising its reliability and modularity. Designing the optimal droop gain to achieve accurate load sharing and effective voltage regulation poses a multi-objective optimization challenge, as these control objectives often conflict with each other. Different artificial intelligence (AI) multi-objective optimization techniques have been employed to compute the optimal droop gains of the converters to achieve the desired control objectives [3, 4, 5, 6, 7, 8, 9, 10, 11]. The most used AI techniques in power electronics applications are the metaheuristic algorithms (such as genetic algorithm (GA) and particle swarm optimization (PSO)) and the machine learning (ML) techniques (an example is the artificial neural network (ANN)) [12].

In [3, 4, 5, 7], the MOOP is tackled by converting these multiple-objective optimization problems to a single objective (SO) one using a weighted sum method [13]. The PSO technique is employed in [3, 4, 5] for the computation of the optimal droop settings to realize two control objectives of current sharing error minimization and enhanced voltage regulations for various loading conditions of a DC microgrid. In the weighted sum approach, the objective functions are added together with different weights for optimization. However, when one objective is realized, the other objective is degraded due to its conflicting nature. Thus, this requires the knowledge of the optimum weighting factor design to obtain the optimal solution. The tuning of the weighting coefficients is not trivial and is a time-consuming task. In addition, a slight change in the weighing coefficient may result in a large change in the control objectives [8, 10]. Besides, this approach only provides a single solution and is highly dependent on the assigned weights, thus, not providing flexibility to the power system designer [14].

In contrast, authors in [8, 10] solved this MOOP by using an extra compromising step called the fuzzy membership function after deriving Pareto optimal front solutions. For example, to obtain the optimal droop gains for distributed generators (DGs) in an islanded DC microgrid, the nondominated sorting genetic algorithm (NSGA II) was used to generate the Pareto optimal front of the formulated multi-objective optimization (MOO) in [8]. The proposed MOO approach considers the system voltage regulation, improved current sharing among the DGs and minimization of the total loss in the system. The fuzzy membership function is employed to obtain the best-compromised solution from the Pareto optimal front.

Though the population-based methods (especially the GA and PSO) are the most widely used to solve optimization problems in power electronics and allow the user to find good optimal design variables (i.e., have good search capability) [12], however, they are heuristic and have an intensive computational burden [12]. In addition, for every design objective, a new set of simulations are required [15] to find the optimal droop gain. Another drawback includes the possibility of being stuck in the local optimum due to the premature convergence of the results of the optimization [16, 17]. Thus, there is no guarantee that their solutions are globally optimal. Besides, since optimization involves different control objectives, there is a need to formulate the objective function. Furthermore, when a wide operating range is considered, the heuristic methods will need to run many simulations and experimental results which are time-consuming. Thus, limiting their practical implementation in industrial applications that require speed and efficiency [12].

A. Motivation for Using the ANNs

An approach can be considered good for optimal droop gain design if it provides the power system designer with a simple way to obtain the optimum system performance for any design criteria without incurring a huge computational burden in the implementation of the algorithm. In this article, the use of the ANN is proposed for the design and computation of the optimal droop gain of PECs. The ANN can offer the optimal solution by automatically learning the underlying relationship between the model inputs and outputs by using its inherent decision-making feature. Also, unlike the classical and well-known optimization techniques that require an explicit fitness function, the ANN can approximate so many non-linear functions to a high degree of accuracy with little knowledge about the system. As a result, it can be applied to a problem where the fitness function is unknown or difficult to formulate and can generate the optimum solution without trade-offs at a reduced computational burden [18]. In addition, the data collection needs to be carried out only once and not several times as is the case with heuristic methods [19] when a different design objective is considered. These are huge advantages of the use of the ANN in a MOOP. Besides, the ANN is the most widely used AI technique in power electronics control applications [12]. The ANN model has been widely employed in applications that require classification, optimization, and prediction.

In recent years, conventional ANN optimization-based design has been employed for the design and automated selection of some power electronics parameters such as the weighting factor in the cost function of the finite control set model predictive control (FCS-MPC) [15, 20, 21]. In [17], it was used to design and select the parameter of the active disturbance rejection control controller for the dual active bridge converter. In [22], an ANN-aided automated design for the reliability of power electronics systems is proposed. The design and optimization of the DC filter for the MEA distribution system using search and surrogate algorithms are carried out in [23]. In [24], it is used for the design and selection of the optimal weighting factors used for predictive torque control in a motor drive. Similarly, [25] employs it to facilitate the design of optimal droop gain for droop control of parallel-connected PECs in the MEA.

In the conventional ANN optimization-based design [15], [17]-[25], the ANN is trained as a surrogate model offline using data obtained from experiments or a detailed simulation model of the EPS under study. Thereafter, the surrogate model is used to replace the original detailed simulation model in performing

optimization and selection of the desired optimal system parameter. Compared to the met-heuristic optimization techniques, the surrogate model in the conventional ANN optimization-based design can be used in future studies without the need of running the original system model and this saves time. In addition, there is no need to run a new set of simulations for new control objectives within a sub-design space [15]. However, despite the benefits of conventional ANN optimization-based design, it exhibits two main drawbacks that are undesirable in practical implementation. Firstly, after training, the process involves probing thousands or even millions of design points using the surrogate model to find the optimal design point, leading to a substantial increase in computational burden and potentially prolonging the execution time [15]. Secondly, similar to meta-heuristic optimization techniques, it necessitates formulating an objective function and converting the MOOP to a Single-Objective (SO) one using the weighted sum method, which adds complexity to the optimal droop gain design and selection process.

AI techniques can provide adaptive and robust power systems control variables that can respond to changes in system conditions in real-time [12]. In this regard, for ease of implementation, methods are required that have low complexity and computational burden. Due to the drawbacks associated with the meta-heuristic approach and conventional ANN optimization-based design, they not only make the offline design of control parameter complex and computationally intensive, but none of these methods also allow control parameters to be tuned in real-time [26]. Based on the literature reviewed, it is identified that it has become imperative to analyze ANN for droop gain parameters design and computation from the practical implementation perspective.

B. Statement of Contribution

Motivated by the above discussions, this article is an extension of the previous work [27], where detailed analysis, generalized methodology, simulation results and controller hardware-in-the-loop (C-HIL) experimental test validation are considered. In addition, it builds upon our recent research [25], where the conventional ANN optimization-based design is used for offline computation of optimal droop gains of PECs. Unlike the work in [25], the proposed approach eliminates the need for intermediate optimizations by utilizing reverse data training of the ANN to directly predict the optimal droop gain settings. Thus, reducing computational burden and complexity, and enabling real-time tuning of droop gain parameters. The proposed approach represents a significant improvement over the method in [25] and offers several advantages: (1) It is a self-contained application that does not depend on external hardware to set the optimal droop gain of converters in local controllers. This advantage stems from the fact that the ANN is implemented directly within a hardware control platform. (2) Facilitates automatic updates of optimal droop gain settings in local controllers, and ensures quick adaptation to reference changes, thereby achieving the desired control performance. (3) By employing real-time computation of droop gains, this method enhances the overall performance and responsiveness of the control system, making it well-suited for a wide range of applications in power systems.

The trained ANN model can be used offline or implemented in a digital control platform for real-time computation of the optimal droop gains. In the proposed approach, once the training is completed, the power system designer can input the desired control objectives (i.e., a specific design point). The surrogate model can then quickly calculate the optimal droop gains based on these specified objectives. This allows for immediate determination of the optimal droop gains using the surrogate model. The main research contributions in this article are highlighted as follows.

1. The design and validation of a real-time method for the online tuning of the optimal droop gains of parallel-connected converters based on the desired power sharing ratios and voltage regulation references. This approach effectively regulates power-sharing and bus voltage control for droop-controlled converters. To the best knowledge of the authors, this work represents the first attempt to address the real-time tuning of optimal droop gain settings for droop control of parallel connected converters.
2. A detailed comparison between the proposed design strategy and conventional ANN optimization-based design has been performed.
3. Extensive simulations and experiments are conducted to validate the effectiveness of the proposed approach.

The article is structured as follows. Section II introduces the system architecture and provides an analysis of the droop control method along with its challenges. The procedure for the proposed and conventional ANN optimization-based optimal droop gain design strategies is discussed in Section III. In Section IV, the proposed approach is compared and validated against the conventional ANN optimization-based design through simulations. Experimental results validating the proposed approach are presented in Section V. Finally, Section VI concludes the article and outlines potential future research directions.

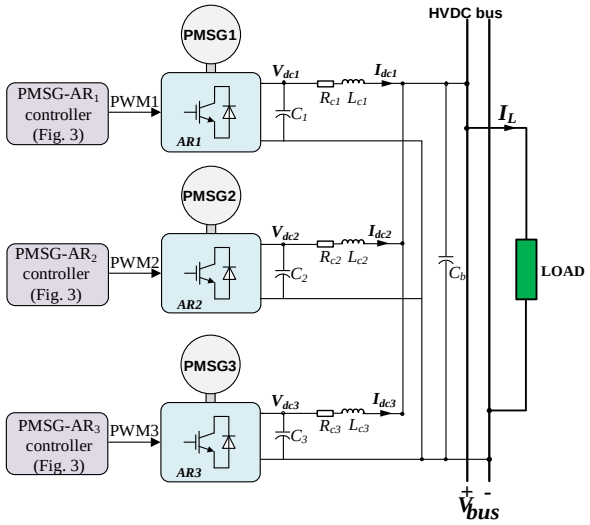

Fig. 2 MEA EPS HVDC grid

II. System Description

A. Islanded DC MG of the MEA EPS

Fig. 2 illustrates the architecture of a 270 V single DC bus power system. This architecture is recognized as a highly prospective choice for the EPS of future more electric aircraft (MEA) [28, 29, 28]. Therefore, it serves as a relevant case study in this article. In Fig. 2, the power system configuration consists of multiple parallel-connected generators (specifically, permanent magnet generators, denoted as PMSGi) that supply electrical power to a high-voltage direct current (HVDC) bus. Each generator is connected to the bus through its respective AC/DC converter (ARi). The chosen converter is a standard two-level voltage source converter, which simplifies the system design and control process. The generators are operated using vector control and are set to operate in the flux weakening (FW) mode at high speeds. The FW control is implemented to ensure that the generators operate within the voltage limit circle as defined in [29]. For more detailed information regarding the control structure of the MEA EPS and design analysis, please refer to [30]. However, the control structure of the system typically follows a cascaded design, consisting of outer voltage and inner current control loops, as depicted in Fig. 3. The outer loop is responsible for regulating the DC-link voltage, which is achieved through the implementation of droop characteristics during the generation mode. On the other hand, the inner current control loop is dedicated to controlling the d- and q-axis currents. The FW controller generates the I_{dref}, while the I_{qref} is produced by the DC-link voltage controller. However, to simplify the control structure and given the focus of this article on the design of droop gains for power sharing among various power generation sources in an onboard HVDC power network for MEA applications, only the droop control structure is presented in Fig. 3.

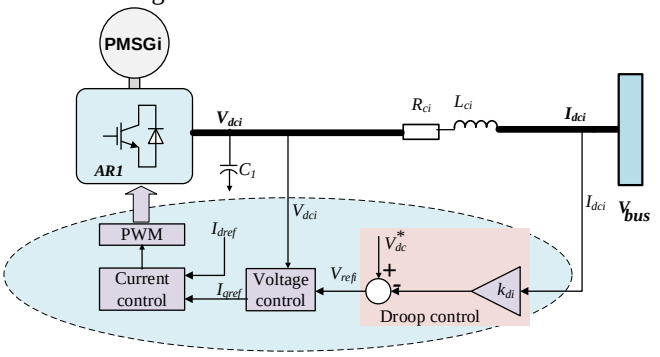

Fig. 3 Local *PMSG-AR$_i$* primary controller

The converters are pulse-width modulated and controlled via their respective primary local controllers. The capacitor C_b is the capacitor bank of the main DC bus, and the local capacitors for each of the converter modules are represented as C_1, C_2 and C_3. The load power in the MEA DC grid is composed of a combination of constant impedance load, such as the wing ice protection load, and constant power load, which is typically driven by tightly controlled power electronics converters like the power converter-driven compressors for the environment control system [31]. For this study, a DC bus load in the form of an inverter-controlled permanent magnet machine (PMM) acting as a constant power load (CPL) is utilized. Additionally, to represent the generators on the left-wing engine, right-wing engine, and auxiliary power unit (APU) of the aircraft, three Permanent Magnet Synchronous Generator (PMSG)-Active Rectifier (AR) systems are considered.

B. Droop Control Method

Within an islanded DC MG, the primary controller is used for current loop and voltage loop control within a single PMSG-AR system. The droop control is generally implemented to define the voltage reference within the primary level voltage control, as shown in Fig. 3. With well-designed current and voltage control, each converter should be able to track its dc-link voltage reference. The generated voltage reference from the droop characteristics can be expressed as

$$V_{ref\,i} = V_{dc}^* - k_{d\,i} I_{d\,ci} \qquad i = 1,2,3 \tag{1}$$

where the droop gain is represented by k_{di}, V_{dc}^* is the nominal DC voltage, and the output currents of the converter are denoted as I_{dci}.

Also, the DC bus voltage connecting the parallel sources from Fig. 3 can be expressed as

$$V_{bus} = V_{refi} - R_{ci} I_{d\,ci} = V_{dc}^* - (k_{di} + R_{ci}) I_{d\,ci} \tag{2}$$

where R_{ci} is the line resistance. In the low-voltage DC MG, the transmission line impedance is predominantly resistive, thus, the line inductance L_{ci} can be ignored. The normalized bus voltage V_{bn} can be obtained by diving V_{bus} by 270.

To limit the bus voltage V_{bus} within an acceptable range, the value of the droop gain is conventionally designed following the expression in (3).

$$k_{di} \le \frac{\delta V_{\max}}{I_{d\,ci\,\max}} \tag{3}$$

where I_{dcimax} is the maximum output current of the converter, and δV_{max} denotes the maximum permissible deviation of the DC bus voltage. The value of δV_{max} is typically set at about 5% of the nominal DC voltage [4]. For the MEA EPS application, a voltage range of between 250 V and 280 V is acceptable in steady states.

From (2), the sharing ratio between the *i*th converter and converter 1 (considered as the base converter) can be expressed as

$$n_1 = \frac{I_{dc2}}{I_{dc1}} = \frac{k_{d1} + R_{c1}}{k_{d2} + R_{c2}} \tag{4}$$

$$n_2 = \frac{I_{dc3}}{I_{dc1}} = \frac{k_{d1} + R_{c1}}{k_{d3} + R_{c3}} \tag{5}$$

where n_1 represents the current sharing ratio between converter 1 and converter 2, while n_2 represents the current sharing ratio between converter 1 and converter 3.

From (4) and (5), the line impedance between generator-connected ARs and the main DC bus has a significant impact on power sharing between different sources. This is extremely true for aerospace applications, where two main generators and PECs (assuming AR1 and AR2) are located within the engine nacelle and another generator set (assuming to be AR3) is

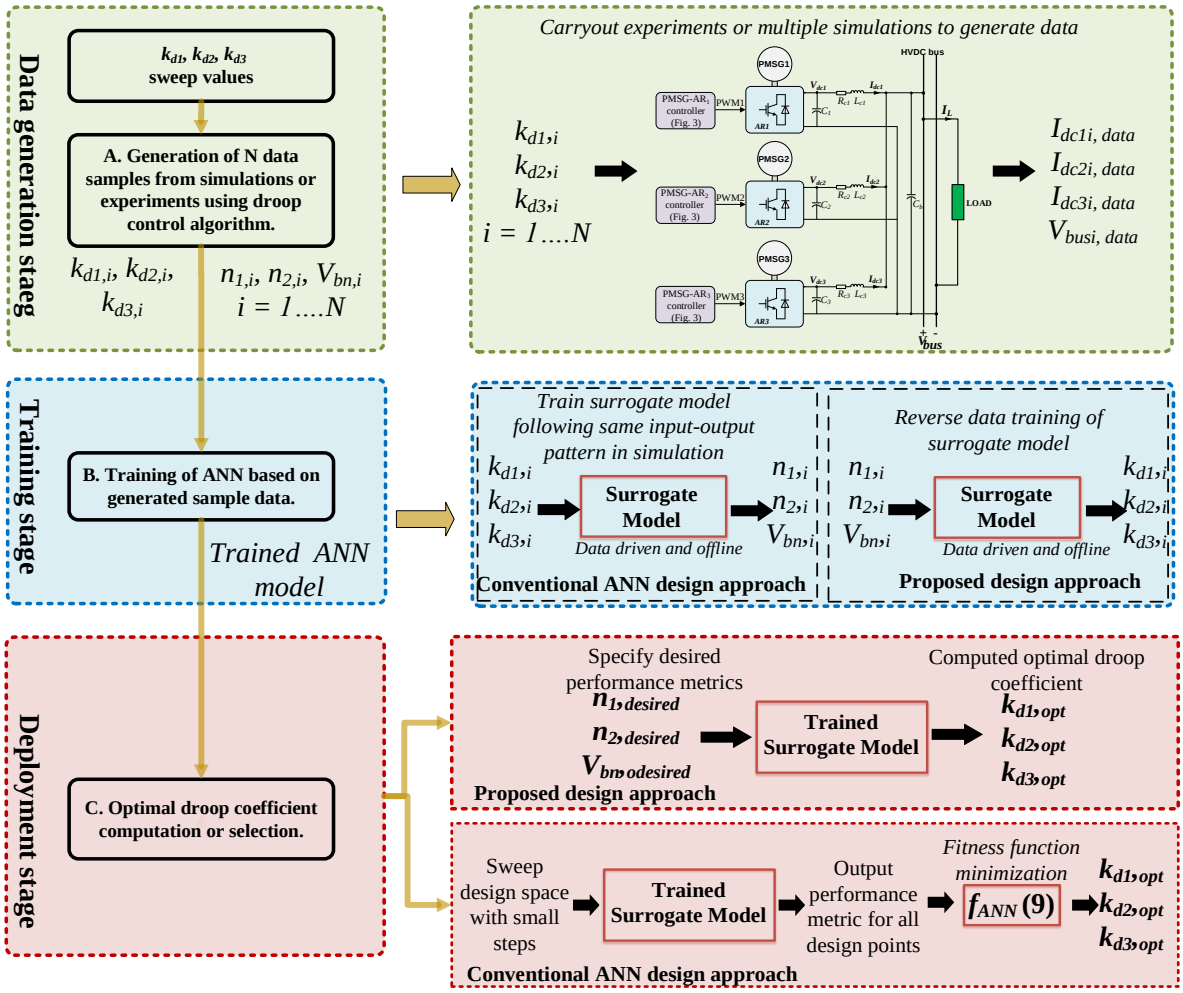

Fig. 4 Flowchart of the comparison of the proposed design approach and conventional ANN optimization-based design of the droop coefficient in droop control of power converters

within the auxiliary power unit located at the tail of the aircraft. These 3 ARs are connected to DC bus bars located at the power distribution center at the center of an aircraft fuselage with long cables. Achieving equal power sharing and maintaining DC bus voltage regulation poses a significant challenge for the droop control method. One approach to ensure accurate power sharing is by setting the droop gains to values much larger than the line resistances (i.e., $k_{di} >> R_{ci}$). By doing so, the power sharing accuracy improves as the influence of line impedance is mitigated. However, the application of large droop gain will compromise the bus voltage regulation as a small load current I_{dci} will result in a large voltage drop V_{dci}.

This article thus proposes a more effective way to enable accurate power sharing and acceptable voltage regulation while mitigating the impact of line impedance with the methodology discussed in Section III.

III. Proposed Droop Gain Design Approach and Comparison with Conventional ANN Optimization-Based Design

This section presents a detailed description of the procedures involved in the droop gain design using both the proposed design approach and the conventional ANN optimization-based design. Additionally, a comprehensive overview of the ANN structure and training process is provided, highlighting the key aspects of the network architecture and the training procedure.

A. Procedure

The design process for both approaches is carried out in three stages, (i.e., Stages A, B and C) as illustrated in the flowchart shown in Fig. 4. Stage A is data generation, and the process is the same for both approaches. The data can be generated from either a detailed simulation or experiments. The data generated from high-fidelity simulation models of a multi-generator system (the system in Fig. 2 as an example) can be carried out on a standard multi-core personal computer (PC). Stage B involves ANN training with the data obtained from stage A in both approaches. The training process varies between the two approaches. With the surrogate model from stage B, the required droop gains can be derived immediately for the defined power sharing ratio and DC bus voltage in stage C using the proposed approach. However, the selection of the optimal droop gain with the aid of the surrogate model from stage B requires extra effort when using the conventional ANN optimization-based design. Hence, the method of obtaining the

optimal droop gain settings differs between the two approaches. These three stages are further elaborated as follows.

In stage A, data is extracted by running the detailed simulation model of the MEA EPS shown in Fig. 2 for different combinations of the droop gains (i.e., k_{d1}, k_{d2}, and k_{d3}) within a design range. The corresponding current sharing ratios (i.e., n_1 and n_2) and the normalized bus voltage (V_{bn}) are computed automatically at the end of each simulation and stored. The relationship between the input (x) and the processed output (y) of the simulation during data generation is represented as [25]

$$y = F(x) \Leftrightarrow (n_1, n_2, V_{bn}) = F(k_{d1}, k_{d2}, k_{d3}) \quad (6)$$

In stage B, for the proposed approach, the surrogate model is trained with the system performance indicators (i.e., n_1, n_2 and V_{bn}) as inputs and the droop coefficients (i.e., k_{d1}, k_{d2} and k_{d3}) as outputs. This way, the surrogate model can be used to predict its output quickly and accurately when provided with a suitable input. For clarity, the surrogate model represents the relationship in (7).

$$y = F(x) \Leftrightarrow (k_{d1}, k_{d2}, k_{d3}) = F(n_1, n_2, V_{bn}) \quad (7)$$

On the other hand, for the conventional ANN optimization-based design, the surrogate model is trained by following the same input-output pattern used in data generation (i.e., the relationship in (6)) to train the surrogate model.

Finally, in stage C, for the proposed approach, the power system designer can specify the desired performance metrics (i.e., one design point) as input for the surrogate model to compute the optimal droop coefficient that will yield such performance as shown in Fig. 4. This approach is expected to significantly reduce the prediction time and simplify the optimal droop coefficient design and computation process. In contrast, the conventional ANN optimization-based design involves a stage C that consists of sampling the design space using small steps, resulting in numerous design points. These design points are then fed into a surrogate model, which predicts the corresponding system performance metrics. Subsequently, a user-defined fitness function, denoted as f_{ann}, is formulated, and evaluated using the surrogate model predictions (refer to Fig. 4). By minimizing the fitness function f_{ann}, the optimal droop coefficient setting that satisfies the desired control objectives can be determined instantly [25].

B. ANN Structure and Training

Theoretical analysis suggests that an ANN has the potential to approximate any input-output relationship with high precision, given the appropriate structure, including the number of neurons and layers, is selected for training. Among the key aspects of structure selection, determining the number of neurons in the hidden layer poses a significant challenge. Typically, this responsibility falls on the power system designer, as it directly impacts the training performance of the ANN. In practice, the structure of the neural network model is often determined through a trial-and-error process, which can be performed rapidly since the training itself takes only a few seconds. A common approach is to start with a small number of neurons in the hidden layer and adjust the count based on the observed training performance [12]. Additionally, the number of neurons in the input and output layers is selected to match the number of input and output variables in the training dataset.

In this article, the surrogate models are trained offline using a feedforward neural network (FFNN) with a Levenberg-Marquardt-based backpropagation training algorithm. The choice of FFNN is driven by its simple structure. In an FFNN, data flows in a forward direction, starting from the input layer and progressing through the hidden layer(s) before reaching the output layer [32]. The FFNN comprises an input layer for processing input data, a hidden layer, and an output layer responsible for generating results, such as predictions or classifications. Neurons within each layer are connected to neurons in the preceding layer through weighted connections. Additionally, a non-linear function is applied to the weighted sum of inputs received by each neuron in the hidden layer, with the output then passed on to the next layer. Depending on the complexity of the problem, the FFNN structure can be expanded to include multiple hidden layers. For a more comprehensive understanding of the FFNN, refer to [18] for additional details. Figs. 5(a) and 5(b) illustrate the structure of the surrogate models for the proposed approach and the ANN optimization-based design, respectively. Both surrogate models consist of three layers. To ensure a fair comparison, both approaches employ hidden layers with 11 neurons each.

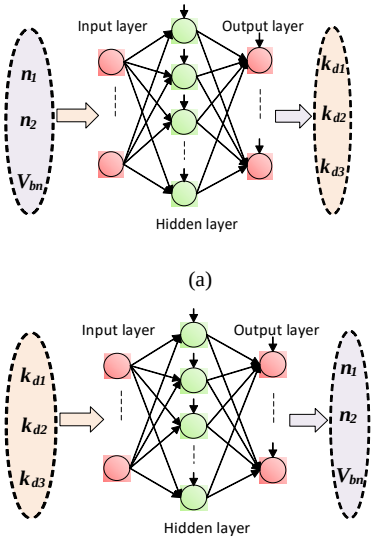

Fig. 5 Schematics of the feed-forward neural networks specifically designed for the computation or selection of the optimal droop gain settings (a) Proposed design approach (b) Convectional ANN optimization-based design [25].

The data sample is divided into three sets—training samples, validation samples, and testing samples—prior to training the surrogate model. The percentage for each set is randomly allocated with the training data having the largest share. Thereafter the weight and biases of the ANN are also randomly selected for the initial iteration. However, the weight and biases are updated in subsequent iterations based on the error observed in the previous iteration. The validation set of data is used to evaluate the ANN training by computing the error between the ANN-predicted output and the training data set [33]. The root mean square error (RMSE) is commonly employed as a metric to assess the training performance of the regression ANN. If the

computed RMSE indicates overfitting or underfitting, the training can be halted. However, if the training performance is unsatisfactory, adjustments can be made to the surrogate model structure, particularly regarding the number of neurons in the hidden layer. For further details on the ANN training algorithm, refer to [34].

IV. Droop Gain Design for the MEA EPS

This section aims to validate the procedures of both design strategies in the context of droop control for the system depicted in Fig. 2. Furthermore, the verification will include the demonstration of Stage C using a design example for both approaches. Additionally, the flexibility of the proposed approach will be showcased through two other design examples. It is worth noting that the proposed design strategy can be applied to other bus systems without any loss of generality, highlighting its broad applicability.

TABLE I
RANGE AND SAMPLING STEP USED IN DATA GENERATION

Parameter	Range	Sampling Step	Number of Samples
$1/k_{d1}$	[3.825, 4.675]	0.085	11 x 11 x 11 = 1331
$1/k_{d2}$	[3.825, 4.675]	0.085	
$1/k_{d3}$	[3.825, 4.675]	0.085	

TABLE II
PARAMETERS OF THE SYSTEM USED AS CASE STUDY IN SIMULATIONS AND EXPERIMENTS

Category	Parameters	Values
PMSG parameters	Nominal power	45 kW
	Base speed	8000 rpm
	Switching frequency f_c	100 kHz
	Maximum modulation index	0.9
	Pole pair	3
	Stator winding resistance R_s	1.058 mΩ
	Winding inductance L_d=L_q	99 µH
	Flux linkage	0.03644 Wb
Converter, cable, and load parameters	DC-link capacitance C_b	1.2 mF
	Converter dead time T_d	3 µs
	DC link-rated voltage	270 V
	Traditional droop coefficients k_{d1}, k_{d2}, and k_{d3}	1/4.25, 1/4.25, 1/4.25
	Cable resistances R_{c1}, R_{c2}, and R_{c3}	3 mΩ,30 mΩ, 15 mΩ
	Cable inductances L_{c1}, L_{c2}, and L_{c3}	1µH, 10 µH, 5 µH

A. Data generation

Prior to data generation, it is important to establish a defined range, known as the design space, for the droop gains. TABLE I presents the range of droop gains used for data generation, along with the corresponding sampling step. The design space is carefully chosen to align with practical considerations, taking into account the desired control objectives while ensuring system stability. In the case of conventional droop gain design, the determination of droop gains is typically based on the power rating of the converters, aiming to achieve effective voltage regulation and stable operation. To maintain consistency, the upper and lower boundaries of the design range for each design parameter are set at +10% and -10% respectively, relative to the conventional droop gains specified in TABLE II. In addition, extensive stability analysis of droop control approaches in voltage source converter-based DC microgrids, along with the investigation of the effects of droop gains on stability [35], confirms that the selected design range falls within the acceptable limits for stable operation. As indicated in TABLE I, a total of 1331 droop gain combinations are systematically explored as inputs in the simulation model depicted in Fig. 2. Random combinations of these inputs are utilized to generate the dataset used for training the artificial neural network (ANN). Following each simulation, the values of n_1, n_2, and V_{bn} are automatically calculated and stored for further analysis.

The simulation utilizes the system parameters and equivalent DC cable parameters listed in TABLE II. The PMSG parameter values in TABLE II are based on the specifications of the AEGART (Aircraft Electrical Starter-Generation System with Active Rectification Technology) machine, designed for the next-generation business Jet application [36]. These PMSGs have identical power ratings and are designed to transmit power in a 1:1:1 ratio. The AC-DC converter's switching frequency, f_c, is set at 100 kHz. To simulate real-world conditions, a dead time T_d and a computational delay of one sampling time are included in the simulation model. The simulations were performed on a standard PC equipped with a quad-core processor, with each simulation taking approximately 6 seconds to execute. Therefore, the total time required for data collection amounts to approximately 35 minutes. The data generation process is automated through MATLAB codes. Data was extracted specifically for a 40-kW load connected to a CPL. The extracted data was subsequently utilized to train the FFNN structures illustrated in Fig. 5 (a) and (b).

B. Development of the Surrogate Model

Prior to training the surrogate models, the generated data is divided into three sets: 70% for training, 15% for validation, and the remaining 15% for testing. The training process is successfully conducted using the NN fitting toolbox in MATLAB. The weights and biases of both surrogate models are optimized using the Levenberg-Marquardt backpropagation algorithm, ensuring a fair comparison between the two approaches. Since the ANNs in the proposed approach and the conventional ANN optimization-based design are trained differently, it is crucial to compare the performance of the ANN models. Fig. 6(a) and Fig. 6(b) illustrate the performance comparison for the two models, where evaluation metrics such as root mean square error (RMSE) and correlation coefficient (regression R-value) are employed. A lower RMSE value and a higher R-value indicate higher accuracy in the trained network predictions. Thus, the closer the RMSE value is to 0 and the R-value is to 1, the better the accuracy of the trained network

predictions.

The proposed approach demonstrates calculated root mean square error (RMSE) values of 0.0032956, 0.002183, and 0.0031714 for k_{d1}, k_{d2}, and k_{d3}, respectively. On the other hand, the conventional ANN optimization-based design approach yields calculated RMSE values of 0.00085733, 0.0012517, and 0.000045932 for n_1, n_2, and V_{bn}, respectively. These RMSE values indicate that the surrogate models are effectively trained, and the FFNN structures presented in Fig. 5(a) and (b) deliver exceptional results. The regression plots depicted in Fig. 6, generated by the NN fitting toolbox, display a strong alignment of data points with the linear regression lines for both approaches. Moreover, the R-values exhibited in Fig. 6(a) and (b) confirm the satisfactory training of the surrogate models in both approaches.

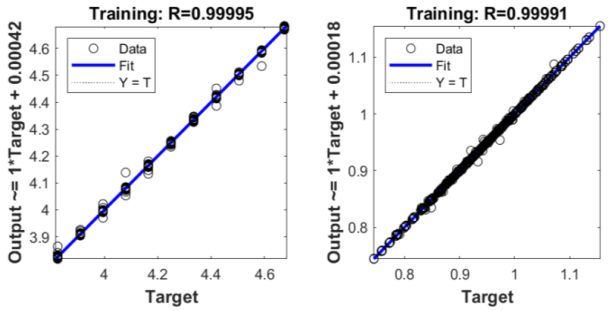

(a) (b)

Fig. 6 Comparison of the regression plot of the trained ANN showing the relationship between the targeted data (o) and the surrogate model prediction (blue line) for (a) Proposed design approach and (b) ANN optimization-based design approach.

C. Design Examples

1) First design example

As the benchmark method, the conventional ANN optimization-based design is initially employed to identify the optimal droop coefficient setting (i.e., k_{d1}^{opt}, k_{d2}^{opt}, and k_{d3}^{opt}) that achieves a well-balanced solution between the current sharing ratios among the converters and normalized bus voltage regulation. Subsequently, the proposed approach is utilized to obtain the same results efficiently and effectively.

a) Conventional ANN optimization-based design

In the initial stage of the conventional ANN optimization-based design, the design range of the droop coefficient is evenly sampled with a small step size of 0.01. This sampling process results in approximately 636,056 design points, representing various droop gains, which are utilized as input for the surrogate model. Subsequently, the surrogate model is employed to predict the corresponding performance metrics, namely n_{1ann}, n_{2ann}, and V_{bnann}, for each of the 636,056 droop gain combinations. These predictions are then utilized to evaluate a user-defined fitness function, facilitating the assessment of the performance of each droop gain setting.

To guide the conventional ANN optimization-based design, a fitness function to achieve the control objective of this design example is formulated as [25]

$$f_{ann1i} = \begin{cases} f_{ann1\_1i} = |n_{1ann} - 1| \\ f_{ann1\_2i} = |n_{2ann} - 1| \\ f_{ann1\_3i} = |V_{bnann} - 1| \end{cases} \quad (8)$$

From (8), three objective functions are defined to quantify the errors in predicted values compared to desired values. Specifically, f_{ann1_1i} represents the error in the difference between the ith predicted current sharing ratio between converters 1 and 2, as estimated by the surrogate model, and the desired current sharing ratio between converters 1 and 2. Similarly, f_{ann1_2i} denotes the error in the difference between the ith predicted current sharing ratio between converters 1 and 3 and the desired current sharing ratio between converters 1 and 3. Finally, f_{ann1_3i} represents the error in the difference between the ith predicted normalized bus voltage (V_{bnann}) and the desired normalized system nominal voltage, set at 1 (i.e., 270 V). Hence, these three objective functions are formulated to assess the discrepancies between predicted and desired values.

To aid in the selection of the optimal design point, the MOOP formulated in (8) is converted to SO using an integrated function as [25]

$$z_i = \sqrt{20.\left(\frac{f_{ann1\_1i}}{f_{ann1\_1max}}\right)^2 + 20.\left(\frac{f_{ann1\_2i}}{f_{ann1\_2max}}\right)^2 + \left(\frac{f_{ann1\_3i}}{f_{ann1\_3max}}\right)^2} \quad (9)$$

It can be observed from (9) that a weighting factor of 20 is assigned to the minimization of the error in the current sharing ratio objective. This choice reflects a higher priority given to this objective over voltage regulation, which is a common practice [4]. The selection of the weighting factor was determined through a trial-and-error process. However, when control objectives have equal priority, a value of 1 can be chosen. To identify the minimum value of e and its corresponding index, an exhaustive search algorithm such as the *min* function in MATLAB can be employed, utilizing the expression provided in (10). Subsequently, this index is used to determine the optimal droop coefficient setting (k_{di}^{opt}) that minimizes the objective function z [25].

$$[\min\_ z, index] = \min(z_i) \quad (10)$$

The evaluation of the expression in (10) using the surrogate model predictions yielded results within approximately 0.16 seconds. The quick execution time highlights the convenience of employing an exhaustive search algorithm to identify the minimum of the fitness function, corresponding to the optimal droop coefficient setting. However, as the system complexity increases, the feasibility of using such an exhaustive search algorithm may diminish. In such cases, the execution time may become impractically long. This topic will be further discussed in Section IV-D to provide more insights.

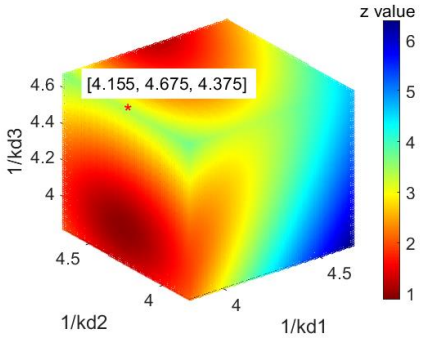

Fig. 7 Plot of the fitness function (9). Optimal droop gain settings were obtained (indicated with the red star).

In Fig. 7, a 3D colour map is presented, depicting the distribution of droop gain design points. The colour of each point corresponds to the value of the integrated function (z) representing the three objectives in equation (9). Based on equation (10), the optimal droop gain design point is selected. In this case, the optimal droop settings are determined as $k_{d1}{}^{opt}$ = 1/4.1550, $k_{d2}{}^{opt}$ = 1/4.6750 and $k_{d3}{}^{opt}$ = 1/4.3750. These optimal values are denoted by a red star marker in Fig. 7. Furthermore, the surrogate model predicts the corresponding current sharing ratios and normalized bus voltage as n_{1ann} = 0.9994, n_{2ann} = 1.0005 and V_{bnann} = 0.9532, respectively.

b) Proposed approach

In the proposed approach, the power system designer is only required to specify the desired system performance metrics within the design space, representing a single design point. These desired metrics serve as inputs to the surrogate model, which computes the optimal droop gain settings necessary to achieve the specified control objectives. To facilitate direct comparison, the predicted performance metrics obtained from the surrogate model in the conventional ANN optimization-based design approach are utilized as inputs for the surrogate model in the proposed approach. Specifically, the desired performance metrics are set as $n_{1desired}$ = 0.9994, $n_{2desired}$ = 1.0005, and $V_{bndesired}$ = 0.9532. As a result, the surrogate model in the proposed approach calculates the optimal droop coefficients as $k_{d1computed}$ = 1/4.1509, $k_{d2computed}$ = 1/4.6718, and $k_{d3computed}$ = 1/4.3710.

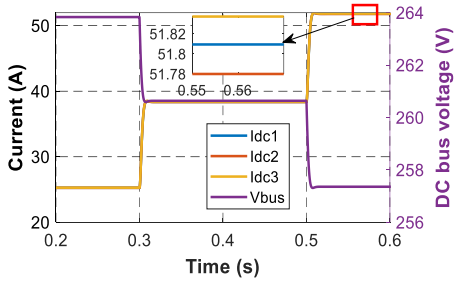

(a)

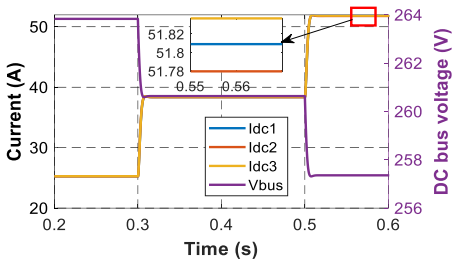

(b)

Fig. 8 Simulation results of a comparison of the current sharing and bus voltage regulation performance using droop gain settings from the (a) Conventional ANN optimization-based design *and* (b) Proposed design approach.

To validate the obtained results, the optimal droop coefficient settings from both approaches are utilized as inputs in the simulation model shown in Fig. 2. Simulations are conducted with different constant power loads (CPLs) of 20 kW, 30 kW, and 40 kW at different time intervals, and the corresponding results are presented in Fig. 8. The simulation parameters remain consistent with those provided in TABLE II. In Fig. 8(a), the current sharing and bus voltage regulation obtained using the optimal droop coefficient settings obtained from the conventional ANN optimization-based design approach are recorded as I_{dc1} = 51.82 A, I_{dc2} = 51.77 A, I_{dc3} = 51.84 A, and V_{bus} = 257.4 V at t = 0.5 s. Consequently, the computed current sharing ratios between the converters and normalized bus voltage regulation are determined as n_1 = 0.9990, n_2 = 1.0004, and V_{bn} = 0.9533. Similarly, in Fig. 8(b), the current sharing and bus voltage regulation using the computed optimal droop coefficient settings from the proposed approach yield I_{dc1} = 51.81 A, I_{dc2} = 51.78 A, I_{dc3} = 51.84 A, and V_{bus} = 257.4 V, respectively. Consequently, the calculated current sharing ratios between the converters and normalized bus voltage regulation are determined as n_1 = 0.9994, n_2 = 1.0006, and V_{bn} = 0.9533.

Based on the obtained results, it is evident that both approaches can achieve the desired control objectives. Additionally, it is observed that under the same design criteria, similar optimal droop gain settings can be obtained from both approaches, resulting in similar control performance as shown in Fig. 8. However, the proposed approach offers notable advantages over the conventional ANN optimization-based design. With the proposed approach, only a single desired design point is required as input to the surrogate model for computing the optimal droop parameters. In contrast, the conventional ANN optimization-based design necessitates processing and feeding the surrogate model with approximately 636,056 design points to determine the optimal droop gain parameter. Moreover, the proposed approach eliminates the need for formulating objective functions and assigning weighting factors to trade off control objectives, which is required in the conventional approach. As a result, the proposed design approach offers the power system designer a simple, flexible, and efficient method for generating optimal droop gain settings with low complexity and computational burden. These advantages are significant when compared to other optimization techniques.

TABLE III
OTHER DESIGN EXAMPLES

Case	Desired performance metrics	Computed optimal droop gains		
		$k_{d1}^{computated}$	$k_{d2}^{computated}$	$k_{d3}^{computated}$
1	$n_{1desired}$ = 1, $n_{2desired}$ = 1, $V_{bndesired}$ = 0.9532	1/4.1508	1/4.6749	1/4.3685
2	$n_{1desired}$ = 0.8, $n_{2desired}$ = 1, $V_{bndesired}$ = 0.9600	1/5.0684	1/4.5701	1/5.4082

In Case 1, all three sources are assumed to have identical ratings and are expected to cooperate in sharing the load power demand equally. Additionally, the bus voltage should be regulated within an acceptable range for the maximum electrical load considered in this study. As shown in TABLE III, for equal load sharing among the sources, the desired sharing ratio is defined as $n_{1desired}$ = 1 and $n_{2desired}$ = 1. Moreover, the desired bus voltage regulation is around 95% of its nominal value (i.e., $V_{bndesired}$ = 0.9532 = 257.364 V). Using the proposed approach, by inputting the above desired performance metrics into the trained surrogate model, the surrogate model predicts the optimal droop gain settings required to achieve such performance objectives, as shown in TABLE III.

In Case 2, generators 1 and 3 are tasked with sharing an equal load (assumed to have the same ratings), which is higher than the load assigned to generator 2 (assumed to have 80% of the rating of generator 1). To accomplish the desired load sharing and bus voltage regulation, the performance metrics presented in TABLE III are employed as inputs to the surrogate model of the proposed approach. The surrogate model predicts the optimal droop gain settings necessary to achieve the desired performance objectives, as shown in TABLE III. This demonstrates that the same surrogate model can be utilized to compute different optimal droop gain settings to accomplish various control objectives within the design space, eliminating the need for additional simulations. Consequently, our proposed approach offers flexibility and time-saving advantages compared to other optimization techniques such as PSO and GA. Due to limitations in space, the predicted optimal droop settings for Cases 1 and 2, as shown in TABLE III, will be validated only in the experiment.

TABLE IV
COMPARISON BETWEEN THE CONVENTIONAL DROOP GAIN DESIGN, CONVENTIONAL ANN OPTIMIZATION-BASED DESIGN AND PROPOSED DESIGN APPROACH FOR THE DESIGN OF THREE CONTROL VARIABLES, kd1, kd2 AND kd3

Method	Accuracy of power sharing	Complexity of implementation	Code execution time	Potential for online tuning of droop gain parameter
Conventional droop gain design	Low	Low	-	-
Conventional ANN optimization-based design [25]	High	High	-High - Around 0.16 s - Increases with an increase in the number of design variables and may become impractically long.	Not possible [26].
Proposed design approach	High	Low	-Low -Around 0.000135 s - Low prediction time irrespective of the number of design variables.	Good [37, 38, 39, 40].

Furthermore, the proposed approach shows potential for online computation of droop gain parameters due to its low complexity and computational burden, as indicated by existing literature [37, 38, 39, 40]. Previous works that share similarities with the proposed design approach demonstrate reduced iterations for identifying optimal control variables [37], decreased computational burden [38], absence of weighting factor tuning, and short execution time [39, 40]. These features serve as the primary motivations behind the proposed approach. In general, ANN models trained offline can be employed either offline or implemented in a digital microprocessor for online applications [40]. The potential, effectiveness, and flexibility of the proposed approach in the computation of the optimal droop gains of converters are further demonstrated by using two other design examples (presented in TABLE III). These examples also demonstrate how the power system designer can leverage the proposed approach in decision-making about the MG operation. Such decisions may include the best mode of operation that will minimize the system losses and maximize its efficiency. However, such an analysis is not within the scope of this article.

2) Other design examples

For the three-source system examined in this article, there are multiple possibilities for meeting the load power demand. This article focuses on two specific approaches, which are outlined in TABLE III.

D. Computational burden

Both approaches share the same computational burden in data generation. For the three design variables considered in this study (i.e., k_{d1}, k_{d2} and k_{d3}), it took approximately 35 minutes to generate the required data. However, if the number of design

variables is increased to four (e.g., for a system with four PMSG-AR systems) and each variable has 11 settings to be tested, a total of 11^4 = 14,641 data samples would be needed for training. With each simulation taking 6 seconds to run on a standard PC with 4-core processors, it would take around 6 hours to generate the data. Therefore, the offline computational burden in stage A increases exponentially as the number of design variables increases. To mitigate this, one option is to increase the sampling step. Instead of testing 11 combinations for each design variable, a smaller number, such as 10, could be tested. This would reduce the total number of data samples generated to 10^3 = 1000 instead of 1331 for a system with three design variables. However, increasing the sampling step may impact the learning and performance of the neural network model [20]. A better solution is to utilize the parallel computing toolbox in MATLAB. This toolbox enables efficient utilization of the computer's multicore processors. By incorporating a few lines of code, simulations that would typically take days to run can be completed in just a few hours. Furthermore, by employing a PC with a higher number of processors, such as 24-core processors, the data generation process can be significantly accelerated. For instance, the 1331 data samples used in this study could be obtained within approximately 6 minutes on a PC with 24-core processors.

While the NN model itself is computationally lightweight, the computational burden in stage C of the conventional ANN optimization-based design increases with the number of design variables. However, the burden is not as significant as in stage A. For example, for the three design variables considered in this study, the surrogate model can output one design point in approximately 0.252 μs, resulting in the evaluation of all 636,056 design points taking around 0.16 s. The optimal solution is then obtained by simply finding the minimum value of the fitness function plot using the *min* function in MATLAB. However, when the number of design variables increases to four, and the same sampling step of 0.01 is used, approximately 55 million fitness functions need to be evaluated using the surrogate model. This evaluation process takes around 14 s. As a result, the computational burden for fitness function evaluation becomes more intensive. Furthermore, evaluating such large fitness functions using the *min* function in MATLAB may become impractically long, and MATLAB's maximum array size preference could be exceeded due to memory and processing limitations. Consequently, the conventional ANN optimization-based design may impose restrictions on the number of design variables that can be effectively handled. To mitigate the computational burden and overcome the limitation on the number of design variables, the fitness function can be evaluated sequentially, or gradient descent optimization can be employed [15]. However, the latter approach may be prone to getting trapped in local minima. On the other hand, stage C of the proposed approach only requires a single user-defined desired design point as input to predict the optimal droop coefficients. Thus, it maintains a low computational burden regardless of the number of design variables, which is a significant advantage.

TABLE IV provides a summarized comparison between the conventional ANN optimization-based design and the proposed design approach. The proposed approach offers additional advantages, including its potential for real-time tuning of droop gain parameters.

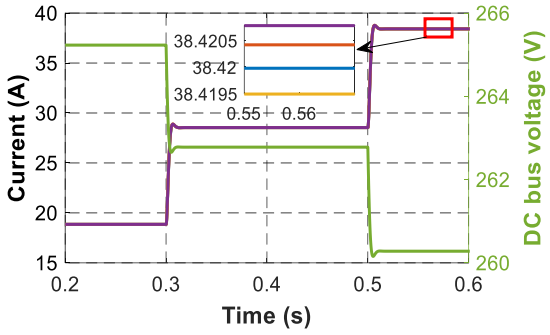

Fig. 9 Simulation results for current sharing and bus voltage regulation using the proposed design approach for equal power sharing among four generators.

E. Equal Power Sharing with Four Generators

To assess the performance of the proposed design approach in scenarios involving more than three control variables, a case study is conducted with four PMSG-AR systems aiming for equal power sharing. In this setup, an additional PMSG-AR system is connected in parallel to the system depicted in Fig. 2. To establish the connection, an extra DC cable with parasitic resistance and inductance values of 20 mΩ and 6.67 μH, respectively, is employed.

To accommodate the additional PMSG-AR system, a new dataset is generated for training the surrogate model. This process involves generating a total of 14,641 data samples, which requires approximately 6 hours to complete. For achieving equal power sharing among the generators and ensuring good bus voltage regulation, the desired inputs provided to the trained surrogate model are specified as $n_{1desired}$ = 1, $n_{2desired}$ = 1, $n_{3desired}$ = 1, and $V_{bndesired}$ = 0.964. Furthermore, the desired current sharing ratio between converter 1 and 4 is denoted as $n_{3desired}$. The surrogate model executes the code and computes the optimal droop gain settings to achieve the desired control performance within a mere 0.000176 seconds.

The computed optimal droop gain settings for the four PMSG-AR systems are determined as $k_{d1}^{computed}$ = 4.0017, $k_{d2}^{computed}$ = 4.4865, $k_{d3}^{computed}$ = 4.2035, and $k_{d4}^{computed}$ = 4.2939. These settings are utilized as inputs in the simulation, where CPLs of 20 kW, 30 kW, and 40 kW are applied at different time intervals. The resulting outcomes are presented in Fig. 9. At t = 0.5 s, the obtained current sharing and bus voltage regulation values are I_{dc1} = 38.42 A, I_{dc2} = 38.42 A, I_{dc3} = 38.42 A, I_{dc4} = 38.42 A, and V_{bus} = 260.30 V. Consequently, the computed current sharing ratios between the converters and normalized bus voltage regulation are determined as n_1 = 1.000, n_2 = 1.000, n_3 = 1.000, and V_{bn} = 0.964. These results demonstrate the capability of our proposed approach to handle complex networks and promptly compute the optimal droop gain settings immediately after the training process.

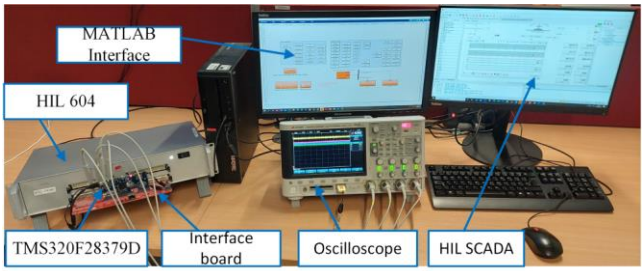

Fig. 10 C-HIL setup

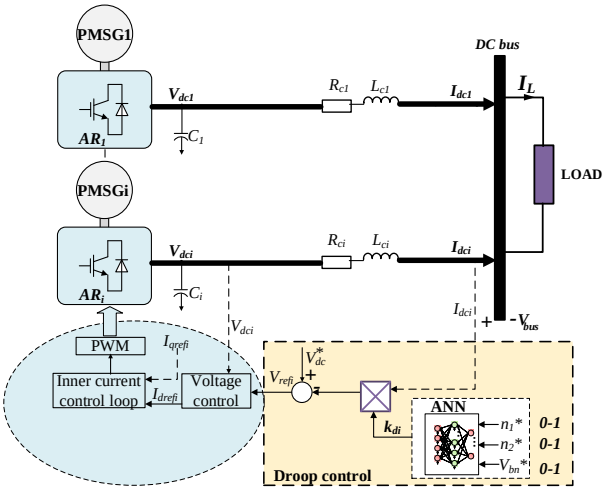

Fig. 11 Block diagram of the proposed control strategy for the PMSG-ARi systems in the MEA EPS distribution network

V. Experimental Results

The proposed ANN-based approach has undergone experimental verification using a controller hardware-in-the-loop (C-HIL) setup, illustrated in Fig. 10, with its corresponding parameters listed in Table II. The primary objective of the study is to achieve real-time computation of the optimal droop gain settings (k_{d1}^{opt}, k_{d2}^{opt}, and k_{d3}^{opt}) for the converters to enable the controller to adapt quickly to reference changes as shown in Fig. 11. As mentioned earlier, the ANN models, trained offline, can be employed either offline or implemented in a digital microprocessor for online applications. The article presents a comparison of the controller's performance using the computed optimal droop gain settings obtained from both the proposed design approach and the conventional ANN optimization-based design. For this comparison, the trained ANN models will be used offline. Hence, the experimental validation section is divided into two parts: validation of the offline computation of optimal droop gain settings using both design approaches and the assessment of real-time implementation performance using the proposed approach.

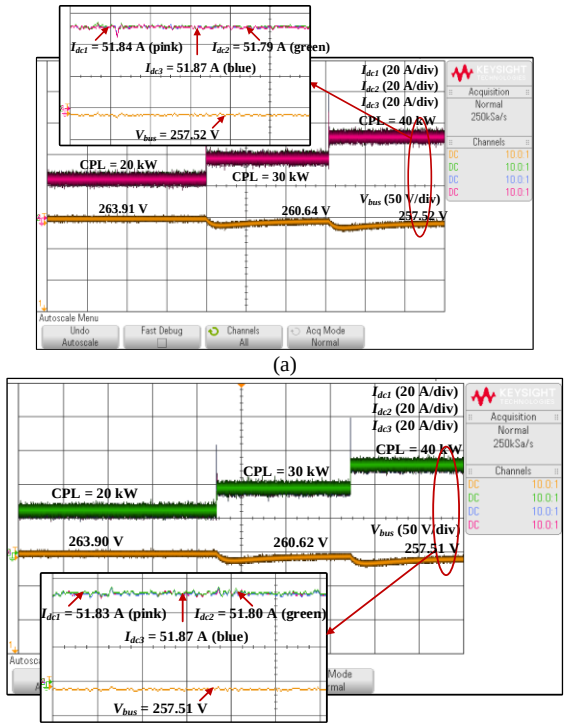

Fig. 12. Comparative Performance Assessment of Current Sharing and Bus Voltage Regulation under Load Changes using Optimal Droop Gain Settings from the First Design Example. (a) Results from Conventional ANN Optimization-Based Design. (b) Results from Proposed Design Approach.

A. *Experimental validation of the offline computed optimal droop gain settings*

In this section, we compare and validate the performance of the controller using the offline computed optimal droop gain settings obtained through both the conventional ANN optimization-based design [25] and the proposed design approach. The C-HIL experimental setup involves modeling the PMSGs, converters, and transmission line impedances from Fig. 2 in real-time and with high fidelity using the typhoon (HIL-604) device real-time emulator. Meanwhile, the control algorithms are implemented on the TI F28379D DSP control card using the Embedded Coder Support Package in MATLAB. The developed codes are debugged and transferred to the DSP through the Code Composer Studio (CCS) software. The gating signal for driving the converter switches is derived from the control card, while communication between the control card and the typhoon software is established through an interface board. Due to the high-fidelity emulation of the power stage by the Typhoon HIL-604 device, the real DSP controller can effectively control the machines and power converters as it would in a physical power stage. This successful integration validates our proposed approach from the controller's perspective. Results collection during the experiments was performed using an oscilloscope.

I. *Load changes*

In this case study, we further validate the optimal droop gain settings obtained from the first design example using both the conventional ANN optimization-based design and the proposed design approach (see Section IV-C) in the Controller Hardware-in-the-Loop (C-HIL) experiment. Additionally, we assess the

current sharing and voltage regulation performance of both approaches when the system experiences load changes. The experimental results are presented in Fig. 12 (a) and (b) for the conventional ANN optimization-based design and the proposed design approach, respectively, with CPLs of 20 kW, 30 kW, and 40 kW applied during the experiment.

Fig. 12 (a) displays the current sharing and voltage regulation results obtained using the optimal droop gain settings from the conventional ANN optimization-based design for the 40-kW load. In this case, the calculated current sharing ratios and normalized bus voltage regulation in steady state are n_1 = 0.9990, n_2 = 1.0006, and V_{bn} = 0.9537, respectively. Similarly, Fig. 12 (b) illustrates the current sharing and voltage regulation results obtained using the computed optimal droop gain settings from the proposed approach for the 40-kW load, resulting in n_1 = 0.9994, n_2 = 1.0008, and V_{bn} = 0.9537 in steady state. These results affirm that both design approaches effectively achieve the desired user-defined control objectives, minimizing the error in current sharing ratios between the generators and ensuring good bus voltage regulation.

Furthermore, it is evident from Fig. 12 (a) and (b) that both design approaches maintain equal current sharing and good voltage regulation even when the load conditions change. This robustness to load changes is a significant advantage of the optimal droop gain design compared to other methods (e.g., adaptive, and non-linear droop control approaches) that require different droop gains for different loading conditions [1, 41].

II. Generator disconnection

In this fault scenario, a constant power load (CPL) of 40 kW is applied during the experiment. The optimal droop gain settings obtained from the first design example are utilized in this scenario (see Section IV-C). Initially, all three *PMSG-AR*$_{1\text{-}3}$ systems work in parallel, sharing the load current demand equally among themselves and regulating the bus voltage as desired (as explained under Scenario I), as shown in Fig. 13 (a) and (b). When the second *PMSG-AR*$_2$ is disconnected (assumed to be under fault), converters 1 and 3 take over the responsibility of supplying the load power demand, as indicated in Fig. 13 (a) and (b). It is observed that there is a drop in the bus voltage for both approaches when *PMSG-AR*$_2$ is disconnected. However, despite the drop in the bus voltage under the fault condition, the bus voltage regulations remain within the acceptable limits (250 V < V_{bus} < 280 V) for the MEA application. Therefore, it can be concluded that both design approaches are robust to generator disconnection and exhibit good and similar transient performance.

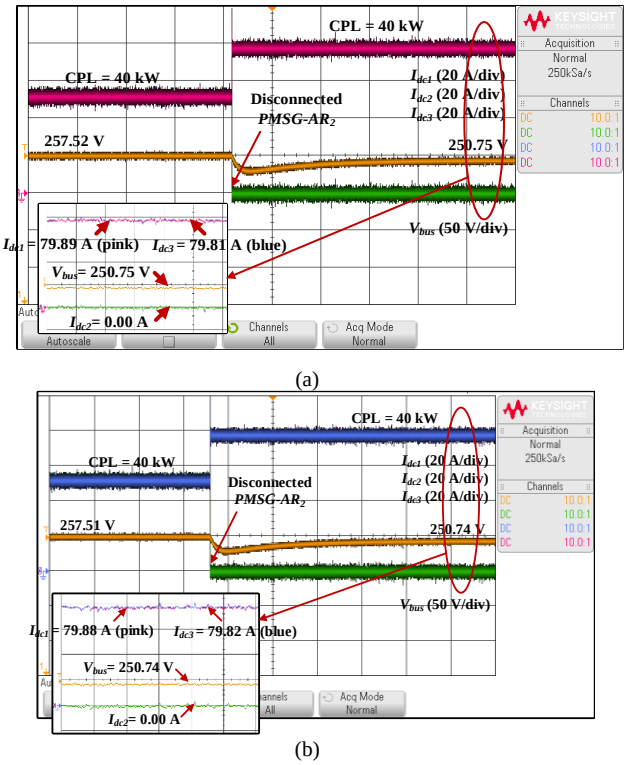

Fig. 13. Comparative Performance Assessment of Current Sharing and Bus Voltage Regulation during Generator Disconnection using Optimal Droop Gain Settings from the First Design Example. (a) Results from Conventional ANN Optimization-Based Design. (b) Results from Proposed Design Approach.

III. Line resistance variation

In this experimental study, the robustness of the optimal droop gain settings obtained using the conventional ANN optimization-based design and the proposed design approach from the first design example (see Section IV-C) is assessed under the scenario where the line resistance values shown in TABLE II are increased by 20%. The experiment is conducted with a 40-kW load, and the results are presented in Fig. 14 (a) and (b) for the conventional ANN optimization-based design and the proposed design approach, respectively.

In Fig. 14 (a), the output currents and bus voltage regulation obtained from the conventional ANN optimization-based design are shown. The calculated current sharing ratios between the converters are n_1 = 0.977 and n_2 = 0.991, resulting in an error of 2.30% and 0.90% in n_1 and n_2, respectively. Similarly, in Fig. 14 (b), the output currents and bus voltage regulation obtained from the proposed design approach are shown. The calculated current sharing ratios between the converters are n_1 = 0.978 and n_2 = 0.991, resulting in an error of 2.20% and 0.90% in n_1 and n_2, respectively. The experimental results demonstrate that both design approaches exhibit a similar and significant reduction in the power sharing error while maintaining the bus voltage regulation within an acceptable range, even in the presence of variation in the line resistance.

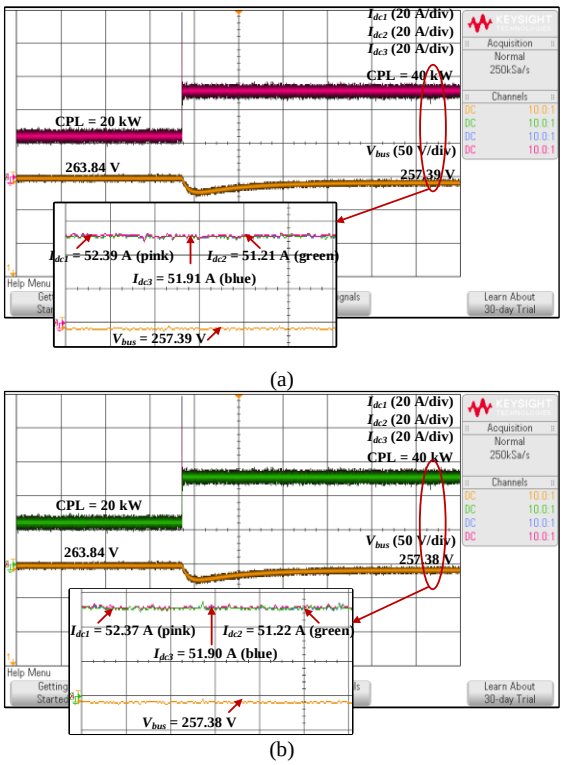

Fig. 14. Comparative Performance Assessment of Current Sharing and Bus Voltage Regulation under Line Resistance Variation using Optimal Droop Gain Settings from the First Design Example. (a) Results from Conventional ANN Optimization-Based Design. (b) Results from Proposed Design Approach.

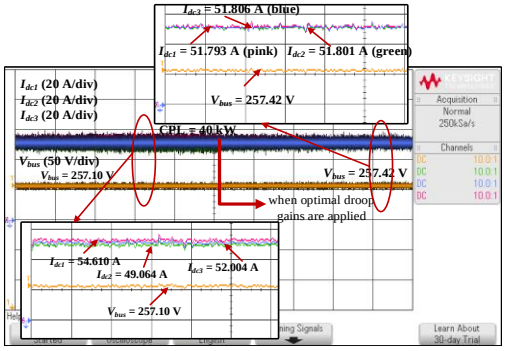

Fig. 15. Comparative Performance Assessment of Current Sharing and Bus Voltage using Different Droop Gain Settings (a) Results with Traditional Identical Fixed Droop Gain Settings (as shown in TABLE II) (b) Results with Optimal Droop Gain Settings for Case 1 from the Other Design Example.

IV. Comparison with conventional droop gain

This test is conducted to compare the current sharing and voltage regulation performance of the conventional droop gain design with the proposed design approach. The parallel-connected PMSG-ARi system shown in Fig. 2 is controlled using two different droop gain settings: traditional identical fixed droop gain settings (as shown in TABLE II) and computed optimal droop gain settings obtained for case 1 (as shown in TABLE III). The experimental results are depicted in Fig. 15, where a CPL of 40 kW is applied during the experiment.

In the conventional droop gain design, the droop gains are identical and determined based on the power rating of the converters (details in Section II). Fig. 15 shows the output currents flowing through the three converters and the bus voltage regulation for the traditional droop gain setting. The calculated current sharing ratios between the converters and normalized bus voltage regulation in steady state are n_1 = 0.8984, n_2 = 0.9523, and V_{bn} = 0.9522, respectively. These results indicate a 10% error in the current sharing ratio between converters 1 and 2, a 4.77% error in the current sharing ratio between converters 1 and 3, and a 4.78% deviation of the bus voltage from its nominal value. These deviations demonstrate that the current sharing using the traditional droop gain settings is not as desired, likely due to the impact of unequal cable resistance on the conventional droop control method. Nevertheless, the bus voltage regulation is within the acceptable range for the MEA application. On the other hand, when the predicted optimal droop gain settings for case 1 are applied, the desired control objectives (as presented in TABLE III) are achieved, and the current sharing and bus voltage regulation improve significantly, as shown in Fig. 15. The calculated current sharing ratio and normalized bus voltage regulation in steady state are n_1 = 1.0002, n_2 = 1.0003, and V_{bn} = 0.9534, respectively.

These results demonstrate a noteworthy enhancement in the current sharing performance of the proposed design approach compared to the conventional droop gain design. The optimal droop gain settings obtained using the proposed approach effectively mitigate the influence of subsystem cable resistance on the current sharing performance of the droop control method. Moreover, it successfully achieves desired system performance without relying on detailed information about the system parameters, such as the corresponding subsystem cable resistance. This effectiveness of the proposed approach is a key motivation of this study, as it enables the quick determination of appropriate droop gain settings for desired control objectives based on sample data collected from a simulation loop, without the need for extensive derivations or detailed information about the system.

V. Unequal power sharing

In this case study, the optimal droop gain settings for case 2, as obtained from the other design examples (see Section IV-C), are validated for unequal power sharing. Fig. 16 displays the current sharing and bus voltage regulation results for the 40-kW load. The computed current sharing ratios and normalized bus voltage regulation in steady state are n_1 = 0.8058, n_2 = 1.0024, and V_{bn} = 0.9592, respectively. These performance metrics closely match the desired control performance used as input to the surrogate model (as shown in TABLE III). Hence, it is confirmed that the proposed design approach can effectively share the load current demand and regulate the bus voltage based on user-defined design criteria.

Furthermore, this validation demonstrates that when a different design criterion is considered within the considered design space, the proposed design approach can directly compute the optimal droop gain settings without requiring another round of data collection, as might be the case with heuristic methods [19]. This highlights the flexibility and efficiency of the proposed design approach, enabling quick

adaptation to various control objectives without the need for additional data gathering or extensive trial-and-error iterations.

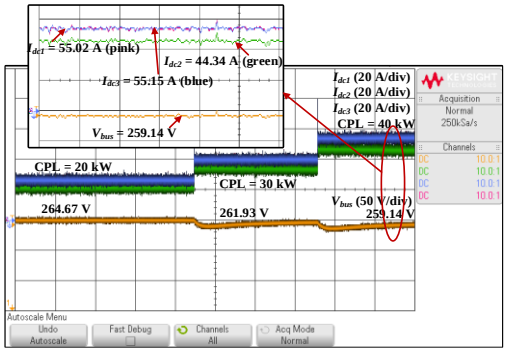

Fig. 16. Experimental results demonstrating unequal current sharing and bus voltage regulation using the optimal droop gain settings from Case 2.

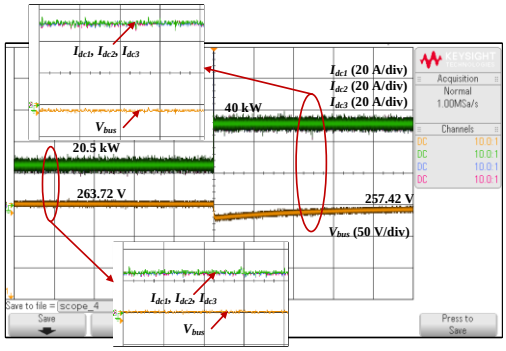

Fig. 17. Experimental results for current sharing and bus voltage regulation using the optimal droop gain settings from Case 1. Response to 20% reduction in C_b (dc-link capacitance).

VI. Robustness to model parameter variation

The experiment is conducted to assess the robustness of the optimal droop coefficient settings obtained using the proposed design approach to variations in the internal model parameters of the system. Specifically, the value of the dc-link capacitance, as shown in Table II, is reduced by 20%. Additionally, a load change from 20.5 kW to 40 kW is applied during the experiment. Fig. 17 displays the results using the optimal droop coefficient settings from case 1.

It can be observed that the optimal droop gains remain robust to parameter uncertainties, with the reduction in capacitance mainly affecting the output DC current of the converters. This is evident from the slight oscillations observed in Fig. 17. Despite these oscillations, the current sharing and bus voltage regulation remain stable and as desired. The experiment validates that the proposed design approach can maintain the desired control performance even in the presence of parameter variations, highlighting its effectiveness and resilience in practical applications.

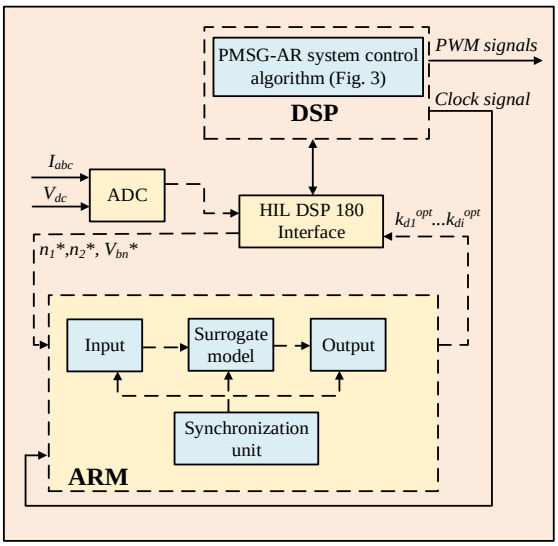

Fig. 18. Block diagram of the proposed approach for the real-time tuning of the optimal droop gains.

B. Evaluation of Real-Time Implementation Performance

I. Digital Implementation

Prior to assessing the real-time implementation performance, this section presents an overview of the digital implementation process. Power system designers leverage the capabilities of Field Programmable Gate Arrays (FPGAs) and advanced Reduced Instruction Set Computing (RISC) machines (such as ARM processors) as these technologies enable the implementation of machine learning algorithms and real-time tuning of control variables (an example is the weighting factor for the FCS-MPC) [26], [42], [43]. ARM refers to a family of processors known for their power efficiency and widespread use in various applications, including mobile devices and embedded systems. They are commonly found in control and communication systems [44].

Fig. 18 shows the block diagram of the procedure for the real-time tuning of the optimal droop gains. As shown in Fig. 18, the PMSG-AR systems control algorithm is implemented and runs on the DSP F28379D control card, while the ANN model's compiled C code runs on the HIL's ARM (ARM Cortex A9) real-time processor [45]. In the C-HIL configuration, real-time tuning of optimal droop gain settings is achieved through the ARM-based implementation of the ANN model. The ARM processor efficiently runs the ANN algorithm, providing rapid and accurate predictions of the optimal droop gain settings. The ANN model, trained offline in MATLAB, is compiled into a Simulink block, and then converted into a Functional Mock-up Unit (FMU) file, including its C source code. This FMU contains the ANN model's mathematical representation, including weights, biases, and activation functions. The inclusion of C source code in the FMU is important for real-time tuning of optimal droop gain in the Typhoon HIL toolchain [46]. Consequently, the ANN model's FMU file is integrated into the Typhoon HIL toolchain via a Functional Mock-up Interface (FMI), allowing the ARM processor to execute the ANN model and making it accessible to the DSP control card for real-time communication through the HIL DSP 180 interface board as shown in Fig. 18. During the C-HIL experiment, the control algorithm running on the DSP control

card continuously interacts with the ARM processor on the Typhoon HIL device to obtain optimized droop gain settings in real-time. This ARM-based implementation ensures low latency, high-speed execution, enabling adaptive control and quick adjustments to the optimal droop gain settings based on user-defined references.

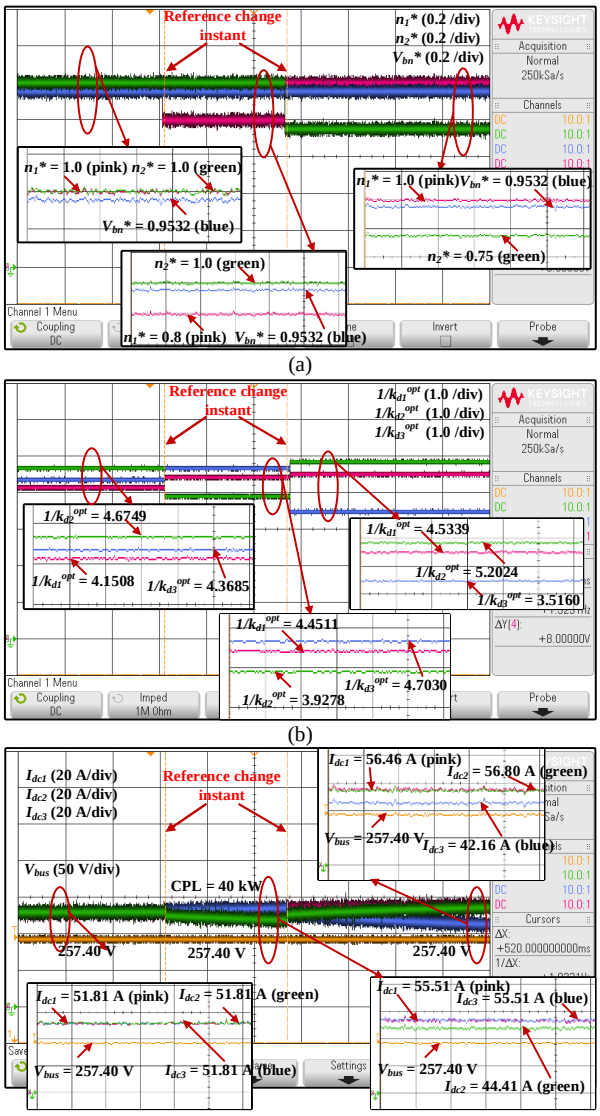

Fig. 19 Transient-state experimental results under CPL = 40 kW. (a) ANN model references: V_{bn}^{*} = 0.9532 (constant), with step changes in current sharing ratios: n_1^{*} = 1.0, n_2^{*} = 1.0; n_1^{*} = 0.8, n_2^{*} = 1.0 and n_1^{*} = 1.0, n_2^{*} = 0.75. (b) Computed optimal droop gain settings by the ANN model (c) Current sharing and bus voltage regulation by the controller.

II. Real-time Assessment Experimental Results

In this section, we experimentally validate the feasibility and effectiveness of our proposed approach for real-time tuning of optimal droop gain settings using the C-HIL setup illustrated in Fig. 10. Firstly, we investigate the transient state performance under varying current sharing ratios while maintaining constant voltage regulation references. A CPL of 40 kW was applied during the experiment. Fig. 19 (a) displays the user-defined references supplied as input to the ANN model. Fig. 19 (b) shows the immediate response of the ANN, continuously updating the computed optimal droop gain settings following each transient. Fig. 19 (c) exhibits the controller's response, adeptly adjusting the current sharing and bus voltage regulation to achieve the desired system responses. Remarkably, the ANN response is nearly instantaneous, presenting a distinctive advantage of the proposed approach compared to alternative solutions based on heuristic and ANN optimization-based design methods. In contrast to those methods, which are confined to the offline computation of the optimal droop gain settings, our approach empowers real-time adaptation and control, enhancing the dynamic performance and responsiveness of the system. Hence, it can be confidently asserted that the proposed strategy functions effectively during transient state operation. In addition, the ANN reliably delivers the correct optimal droop gain settings (k_{di}^{opt}) for each operational point, empowering the controller to achieve the desired system response effectively.

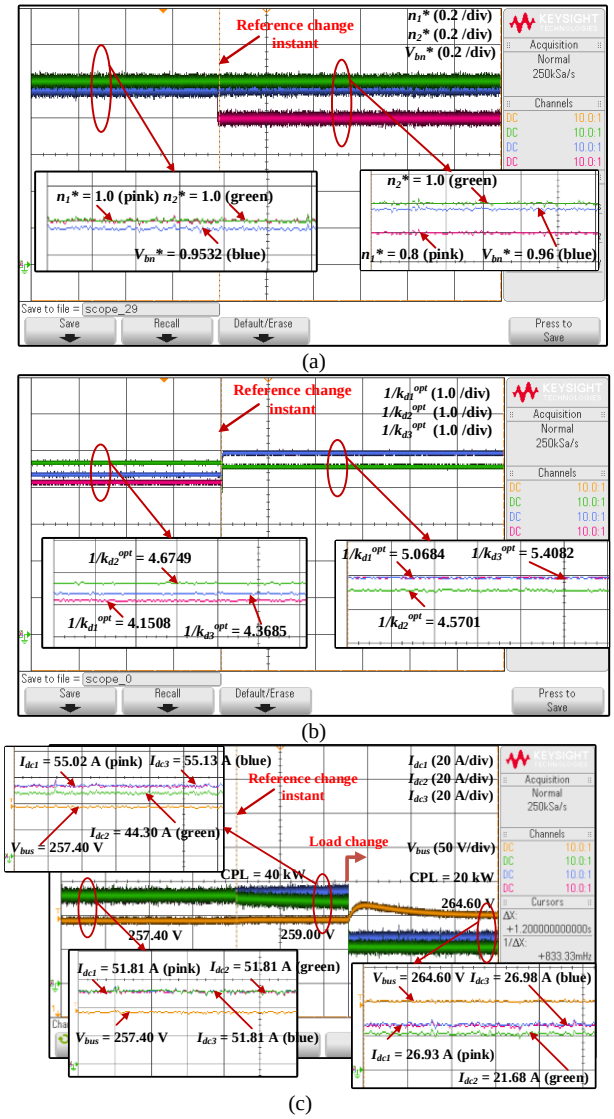

Fig. 20 Transient-state experimental results under CPLs = 40 kW and 20 kW. (a) ANN model references: n_1^{*} = 1.0, n_2^{*} = 1.0, V_{bn}^{*} = 0.9532 with step change of n_1^{*} = 0.8, n_2^{*} = 1.0, V_{bn}^{*} = 0.96. (b) Computed optimal droop gain settings by the ANN model (c) Current sharing and bus voltage regulation by the controller.

Fig. 20 presents the transient experimental results, capturing load changes. Specifically, Fig. 20 (a) illustrates the step change

in the desired system responses, serving as the input to the ANN model. Fig. 20 (b) showcases the corresponding step changes in the computed optimal droop gain settings by the ANN model, responding to the reference modifications. Additionally, Fig. 20 (c) displays the outcomes of current sharing and voltage regulation before and after the applied step-change transient. As depicted in Fig. 20 (c), the controller successfully maintains the desired current sharing ratios between the converters even in the face of load changes. Moreover, the droop control mechanism leads to improved bus voltage regulation as the load power demand decreases from 40 kW (assumed maximum load) to 20 kW. Nonetheless, for the 40-kW power demand, the controller achieves precise bus voltage regulation, following the desired reference. Of particular note, the ANN rapidly and autonomously adjusts the optimal droop gain settings to match the actual operating conditions. Furthermore, through the proposed approach, the controller demonstrates quick adaptability to reference changes, facilitating efficient and accurate control of the system.

VI. Conclusion and Future Work

Existing methods for determining optimal droop gain settings have relied on heuristic approaches and ANN optimization-based design. However, these methods have drawbacks: heuristic optimization requires time-consuming simulation or experimental results for specific design points, while ANN optimization involves processing large datasets to find the best droop gain settings. Consequently, these approaches are complex and time-consuming, hindering real-time tuning of the optimal droop gain settings. To overcome these challenges, this article introduces a fast and real-time method for computing the optimal droop gain settings in the droop control of parallel connected converters. The proposed approach utilizes reverse data training of an ANN, allowing online determination of the optimal droop gain settings based on the power sharing ratio and bus voltage regulation references. The implementation of the proposed design approach on a hardware control platform achieves the desired current-sharing ratios between converters and efficiently regulates the bus voltage, enhancing the overall control performance in real-time. The effectiveness of the proposed approach has been experimentally validated using the C-HIL experimental approach. A detailed comparison between the proposed approach and the conventionally ANN optimization-based design has been performed, which shows the simplicity, flexibility, and low computational burden of the proposed design approach. Due to the real-time implementation of the ANN on a control hardware platform, one potential avenue for future research could involve utilizing the presented approach to create a pre-trained ANN-based surrogate model, which can then be fine-tuned and adapted using online learning techniques. This approach has the potential to accelerate and simplify the process of online training, making it more efficient and effective.

References

[1] S. Augustine, M. K. Mishra and N. Lakshminarasamma, "Adaptive droop control strategy for load sharing and circulating current minimization in low-voltage standalone DC microgrid," *IEEE Transactions on Sustainable Energy*, vol. 6, no. 1, pp. 132-141, January 2015.

[2] J. P. Lopes, C. L. Moreira and A. G. Madureira, "Defining control strategies for microgrids islanded operation," *IEEE Transactions on power systems*, vol. 21, no. 2, pp. 916-924, May 2006.

[3] F. Cingoz, A. Elrayyah and Y. Sozer, "Optimized droop control parameters for effective load sharing and voltage regulation in DC microgrids," *Electric Power Components and Systems*, vol. 43, no. 8-10, pp. 879-889, 2015.

[4] F. Cingoz, A. Elrayyah and Y. Sozer, "Optimized settings of droop parameters using stochastic load modeling for effective DC microgrids operation," *IEEE Transactions on Industry Applications*, vol. 53, no. 2, pp. 1358-1371, March-April 2017.

[5] Shivam and R. Dahiya, "Distributed control for DC microgrid based on optimized droop parameters," *IETE journal of research*, vol. 66, no. 2, pp. 192-203, 2018.

[6] M. Mokhtar, M. I. Marei and A. A. El-Sattar, "Improved current sharing techniques for DC microgrids," *Electric Power Components and Systems*, vol. 46, no. 7, pp. 757-767, 2018.

[7] M. A. Hassan and M. A. Abido, "Optimal design of microgrids in autonomous and grid-connected modes using particle swarm optimization," *IEEE Transactions on power electronics*, vol. 26, no. 3, pp. 755-769, March 2011.

[8] A. M. Dissanayake and N. C. Ekneligoda, "Multiobjective optimization of droop-controlled distributed generators in DC microgrids," *IEEE Transactions on Industrial Informatics*, vol. 16, no. 4, pp. 2423-2435, April 2020.

[9] K. Yu, Q. Ai, S. Wang, J. Ni and T. Lv, "Analysis and optimization of droop controller for microgrid system based on small-signal dynamic model," *IEEE Transactions on Smart Grid*, vol. 7, no. 2, pp. 695-705. doi:10.1109/TSG.2015.2501316, March 2016.

[10] V. V. Thanh and W. Su, "Improving current sharing and voltage regulation for DC microgrids: A decentralized demand response approach," *IEEE Transactions on Smart Grid*, 2022.

[11] I. Y. Chung, W. Liu, D. A. Cartes, E. G. Collins and S. I. Moon, "Control methods of inverter-interfaced distributed generators in a microgrid system," *IEEE Transactions on Industry Applications*, vol. 46, no. 3, pp. 1078-1088, 2010.

[12] S. Zhao, F. Blaabjerg and H. Wang, "An overview of artificial intelligence applications for power electronics," *IEEE Transactions on Power Electronics*, vol. 36, no. 4, pp. 4633 - 4658, 2021.

[13] L. Zadeh, "Optimality and non-scalar-valued performance criteria," *IEEE transactions on Automatic Control*, vol. 8, no. 1, pp. 59-60, 1963.

[14] K. Deb, *Multi-objective optimisation using evolutionary algorithms: an introduction. In Multi-objective evolutionary optimisation for product design and manufacturing*, London: Springer, 2011.

[15] T. Dragičević and M. Novak, "Weighting factor design in model predictive control of power electronic converters: An artificial neural network approach," *IEEE Transactions on Industrial Electronics*, vol. 66, no. 11, pp. 8870-8880, Nov. 2019.

[16] A. Abraham and S. Das, Eds., *Computational intelligence in power engineering (Vol. 302)*, Springer, 2010.

[17] Y. Zeng, A. I. Maswood, J. Pou, X. Zhang, Z. Li, C. Sun, S. Mukherjee, A. K. Gupta and J. Dong, "Active Disturbance Rejection Control Using Artificial Neural Network for Dual-Active-Bridge-Based Energy Storage System," *IEEE Journal of Emerging and Selected Topics in Power Electronics*, 2021.

[18] B. K. Bose, "Neural network applications in power electronics and motor drives—An introduction and perspective," *IEEE Transactions on Industrial Electronics*, vol. 54, no. 1, pp. 14-33, 2007.

[19] P. Zanchetta, "Heuristic multi-objective optimization for cost function weights selection in finite states model predictive control," in *2011 Workshop on Predictive Control of Electrical Drives and Power Electronics*, pp. 70-75, 2011.

[20] M. Novak, T. Dragicevic and F. & Blaabjerg, "Weighting factor design based on Artificial Neural Network for Finite Set MPC operated 3L-NPC

converter," in *2019 IEEE Applied Power Electronics Conference and Exposition (APEC)*, pp. 77-82, Anaheim, CA, USA, March 2019.

[21] X. Wang, Y. Gao, J. Atkin and S. Bozhko, "Neural Network based Weighting Factor Selection of MPC for Optimal Battery and Load Management in MEA," in *2020 23rd International Conference on Electrical Machines and Systems (ICEMS)*, pp. 1763-1768, Hamamatsu, Japan, 2020, November.

[22] T. Dragičević, P. Wheeler and F. Blaabjerg, "Artificial intelligence aided automated design for reliability of power electronic systems," *IEEE Transactions on Power Electronics*, vol. 38, no. 4, pp. 7161-7171, August 2019.

[23] Y. Gao, T. Yang, S. Bozhko, P. Wheeler and T. Dragičević, "Filter design and optimization of electromechanical actuation systems using search and surrogate algorithms for more-electric aircraft applications," *IEEE Transactions on Transportation Electrification*, vol. 6, no. 4, pp. 1434-1447, 2020.

[24] M. Novak, H. Xie, T. Dragicevic, F. Wang, J. Rodriguez and F. Blaabjerg, "Optimal cost function parameter design in predictive torque control (PTC) using artificial neural networks (ANN)," *IEEE Transactions on Industrial Electronics*, vol. 68, no. 8, pp. 7309 - 7319, August 2021.

[25] H. Hussaini, T. Yang, Y. Gao, C. Wang, M. Urrutia and S. Bozhko, "Optimal Droop Control Design Using Artificial Intelligent Techniques for Electric Power Systems of More-Electric Aircraft," IEEE Transactions on Transportation Electrification, 2023.

[26] S. Vazquez, D. Marino, E. Zafra, M. Valdes, J. J. Rodriguez-Andina, L. G. Franquelo and M. Manic, "An Artificial Intelligence Approach for Real-Time Tuning of Weighting Factors in FCS-MPC for Power Converters," *IEEE Transactions on Industrial Electronics*, November 2021.

[27] H. Hussaini, T. Yang, Y. Gao, C. Wang, M. A. Mohamed and S. Bozhko, "Artificial Neural Network Aided Cable Resistance Estimation in Droop-Controlled Islanded DC Microgrids," in *IECON 2021–47th Annual Conference of the IEEE Industrial Electronics Society*, pp. 1-7, 2021, October.

[28] F. Gao, S. Bozhko, Y. S. Shen and G. Asher, "Control design for PMM starter-generator operated in flux-weakening mode," in *2013 48th International Universities' Power Engineering Conference (UPEC)*, pp. 1-6), 2013, September.

[29] F. Gao, S. Bozhko, G. Asher, P. Wheeler and C. Patel, "An Improved Voltage Compensation Approach in a Droop-Controlled DC Power System for the More Electric Aircraft," *IEEE Transactions on Power Electronics*, vol. 31, no. 10, pp. 7369 - 7383, 2016.

[30] S. Bozhko, S. S. Yeoh, F. Gao and C. Hill, " Aircraft starter-generator system based on permanent-magnet machine fed by active front-end rectifier," in *IECON 2014-40th Annual Conference of the IEEE Industrial Electronics Society*, pp. 2958–2964, 2014, October.

[31] C. Wang, H. Hussaini, F. Gao and T. Yang, "*Modeling and control of DC grids within more-electric aircraft," in Modeling, Operation, and Analysis of DC Grids*, Academic Press, 2021, pp. 337-366.

[32] M. Naguib, P. Kollmeyer and A. Emadi, "Application of Deep Neural Networks for Lithium-Ion Battery Surface Temperature Estimation Under Driving and Fast Charge Conditions," *IEEE Transactions on Transportation Electrification*, vol. 9, no. 1, pp. 1153 - 1165, March 2023.

[33] S. Skansi, *Introduction to Deep Learning: from logical calculus to artificial intelligence*, Springer, 2018.

[34] T. Guillod, P. Papamanolis and J. W. Kolar, "Artificial neural network (ANN) based fast and accurate inductor modeling and design," *IEEE Open Journal of Power Electronics*, vol. 1, pp. 284-299., 2020.

[35] F. Gao, S. Bozhko, A. Costabeber, C. Patel, P. Wheeler, C. I. Hill and G. Asher, "Comparative stability analysis of droop control approaches in voltage-source-converter-based DC microgrids," *IEEE Transactions on Power Electronics*, vol. 32, no. 3, pp. 2395 - 2415, March 2017.

[36] S. Bozhko, T. Yang, J. M. Le Peuvedic, P. Arumugam, M. Degano, A. La Rocca, Z. Xu, M. Rashed and P. Wheeler, "Development of aircraft electric starter–generator system based on active rectification technology," *IEEE Transactions on Transportation Electrification*, vol. 4, no. 4, pp. 985 - 996, December 2018.

[37] I. Harbi, M. Ahmed, J. Rodriguez, R. Kennel and M. Abdelrahem, "Low-complexity finite set model predictive control for split-capacitor ANPC inverter with different levels modes and online model update," *IEEE Journal of Emerging and Selected Topics in Power Electronics*, vol. 11, no. 1, pp. 506-522, Feb. 2023.

[38] I. Harbi, M. Ahmed, C. M. Hackl, J. Rodriguez, R. Kennel and M. Abdelrahem, "Low-Complexity Dual-Vector Model Predictive Control for Single-Phase Nine-Level ANPC-Based Converter," *IEEE Transactions on Power Electronics*, vol. 38, no. 3, pp. 2956-2971, March 2023.

[39] A. Nasr, C. Gu, G. Buticchi, S. Bozhko and C. Gerada, " A Low-Complexity Modulated Model Predictive Torque and Flux Control Strategy for PMSM Drives without Weighting Factor," *IEEE Journal of Emerging and Selected Topics in Power Electronics*, February 2022.

[40] S. Wang, T. Dragicevic, Y. Gao and R. Teodorescu, "Neural network based model predictive controllers for modular multilevel converters," *IEEE Transactions on Energy Conversion*, vol. 36, no. 2, pp. 1562-1571, June 2021.

[41] F. Chen, R. Burgos, D. Boroyevich, J. C. Vasquez and J. M. Guerrero, "Investigation of nonlinear droop control in DC power distribution systems: Load sharing, voltage regulation, efficiency, and stability," *IEEE Transactions on Power Electronics*, 2019.

[42] H. Bai, C. Liu, E. Breaz and F. Gao, "Artificial neural network aided real-time simulation of electric traction system," Energy and AI, vol. 1, no. 2020: 100010., pp. 1-12, 2020.

[43] I. Harbi, J. Rodriguez, E. Liegmann, H. Makhamreh, M. L. Heldwein, M. Novak, M. Rossi, M. Abdelrahem, M. Trabelsi, M. Ahmed, P. Karamanakos, S. Xu, T. Dragicevic and R. Kennel, " Model Predictive Control of Multilevel Inverters: Challenges, Recent Advances, and Trends," IEEE Transactions on Power Electronics, 2023.

[44] M. D. V. Pena, J. J. Rodriguez-Andina and M. Manic, "The internet of things: The role of reconfigurable platforms," IEEE Industrial Electronics Magazine, vol. 11, no. 3, pp. 6-19, September 2017.

[45] "Typhoon HIL Documentation," Typhoon HIL Inc., [Online]. Available: https://www.typhoon-hil.com/documentation/typhoon-hil-application-notes/References/terrestrial_microgrid_%28switching%29. [Accessed 15 7 2023].

[46] "Typhoon HIL Documentation," Typhoon HIL Inc., [Online]. Available: https://www.typhoon-hil.com/documentation/typhoon-hil-software-manual/References/fmu_import.html#fmi_import__fig_vns_2fd_zvb. [Accessed 15 07 2023].

Habibu Hussaini was born in Minna, Nigeria. He received his B.Eng. degree in Electrical and Computer Engineering from the Federal University of Technology, Minna, Nigeria in 2010. He obtained his MSc. in Energy and Sustainability with Electrical Power Engineering from the University of Southampton, the United Kingdom in 2015. He is currently studying for his Ph.D. in Electrical and Electronics Engineering at the University of Nottingham, United Kingdom. He is a lecturer with the Federal University of Technology, Minna, Nigeria.

His research interests include aircraft electrical power systems, artificial intelligence-based design, control and parameter identification, and power electronics and control.

Tao Yang (Senior Member, IEEE) received the Ph.D. degree in electrical engineering from the University of Nottingham, Nottingham, U.K., in 2013.

Since then, he has been a Researcher with the Power Electronics, Machines and Control Group, University of Nottingham, where he became an Assistant Professor in 2016 and an Associate Professor in 2019. His research interests include high-speed electric motor drive control, power electronic conversion, and electrical system design and optimization for more-electric/hybrid/all-electric aircraft applications

Dr. Yang is a Fellow of IET and Higher Education Academy, and an Associate Editor for the IEEE Transactions on Transportation Electrification and Chinese Journal of Aeronautics.

Ge Bai (Student Member, IEEE) received the M.Sc. degree from the University of Nottingham, UK, in 2021. She is currently working toward the Ph.D. degree in Electrical and Electronic Engineering with the Power Electronics, Machines, and Control Group, University of Nottingham, UK.
Her research interests include high-speed machine drives, advanced integrated power generation center for more-electric aircraft, and dc microgrid stability.

Matías Urrutia was born in Santiago, Chile. He received the BSc and MSc. in Electrical Engineering from Federico Santa Maria Technical University (UTFSM) in 2017. In 2022, Mr. Urrutia obtained a dual-degree PhD in Electrical and Electronic Engineering from the University of Chile and the University of Nottingham. He was a part-time lecturer at the UTFSM Electrical Engineering Department from 2018 to 2021. From May 2021 to March 2023, he worked as a Research Fellow in the PEMC group of the University of Nottingham. Since April 2023, he has been a Senior Power Electronics Engineer at Sprint Electric Ltd, United Kingdom.
His main interests are Modular Multilevel Converters, Matrix Converters, Model predictive Control and modern FPGA-based digital control schemes for power electronics applications.

Serhiy Bozhko (Senior Member, IEEE) received the M.Sc. and Ph.D. degrees in electromechanical systems from the National Technical University of Ukraine, Kyiv, Ukraine, in 1987 and 1994, respectively. Since 2000, he has been with the Power Electronics, Machines and Controls Research Group, University of Nottingham, Nottingham, U.K., where he is currently a Professor of aircraft electric power systems and the Director of the Institute for Aerospace Technology. He is leading several EU- and industry funded projects in the area of aircraft electric power systems, including power generation, distribution and conversion, power quality, control and stability issues, power management and optimization, and advanced modeling and simulation methods.